Changing feeding levels reveal plasticity in elasmobranch life history strategies

Sol Lucas*, Per Berggren, Ellen Barrowclift, Isabel M. Smallegange*

School of Natural and Environmental Sciences, Newcastle University, Newcastle upon Tyne, NE1 7RU, UK

***Author contact:** s.a.lucas2@newcastle.ac.uk, Isabel.smallegange@newcastle.ac.uk

ORCID ID's: Smallegange Orcid: 0000-0001-6218-7358. Lucas Orcid: 0000-0003-2497-7089. Berggren Orcid: 0000-0001-8204-7256. Barrowclift Orcid: 0000-0003-0625-0919.

Abstract

Life history strategies are shaped by phylogeny, environmental conditions and individual energy budgets, and have implications for population performance. Here, we used an approach that merges demography with energy budget theory to structure life history traits of 151 elasmobranch species into life history strategies for two contrasting feeding levels. We assessed how phylogeny and habitat impacted life history strategies, and tested if these strategies predict population performance and conservation status. Elasmobranch life history strategies are structured along the fast-slow continuum and reproductive strategy axes. However, species' positions in this life history space were not fixed, but instead moved in an anticlockwise 'whirlpool' manner along the two axes in response to an increase in feeding level. We also found that population growth rate does not necessarily inform on a species demographic resilience. Finally, only at the higher feeding level does the fast-slow continuum predict IUCN conservation status, with the slowest species at the highest risk of extinction. Our analyses reveal plasticity in species life history strategies, and warn against extrapolating the fast-slow continuum and reproductive strategy framework from one environment to another when predicting a species' response to (climate) change, perturbations, and, particularly in case of elasmobranchs, (over)exploitation.

1. Introduction

Life history strategies of many animals and plants reflect "life history speed" or "pace of life" along a fast-slow continuum, and reproductive biology along a reproductive strategy axis[1–3]. Fast species mature early, grow fast and are short-lived and slow species are slow-growing and long-lived with low fecundity[4]. The reproductive strategy axis is characterised by high lifetime reproductive output and high mortality at one end, and low reproductive output and low mortality at the other[5] (in some studies this second axis relates to development instead[6]). These axes are shaped by trade-offs[4]. For

example, the fast-slow continuum represents the trade-off between reproduction versus survival[6], often irrespective of body size or phylogenetic relatedness[7–9]. Yet, trade-offs that operate within individuals, such as trading off growth versus reproduction in the energy budget[7,8], should be considered, as different dynamics can exist between populations or species with similar traits[10,11]. Specifically, the classical association between life history strategies and population responses to environmental change breaks down when accounting for individual-level trade-offs and energy allocation in ray-finned fish[12]. There is also limited understanding of how ecological and evolutionary factors, like phylogeny or habitat type, shape variation in life history strategies across species[1,2,4,13]. Identifying patterns in life history strategies across the tree of life is essential to predicting population growth rates and demographic resilience (herein 'population performance')[2]. However, to do so requires in-depth understanding of how energy budgets, phylogeny and habitat structure life history strategies across species[1,13,14].

Elasmobranchs (sharks, skates and rays) encompass a vast amount of life history variation. Longevity, for example, can range from five (e.g. *Carcharhinus sealei* and *Carcharhinus sorrah*[15]) to almost 400 years (*Somniosus microcephalus*[16]). Reproduction is highly variable, including oviparity (skates and three families of shark), aplacental viviparity (in various forms; sharks and rays) and placental viviparity (some sharks)[17,18]. Elasmobranch population performance typically varies with body size, reproductive strategy and environmental temperature[19–21], yet little is known about the impact of energy budgets. Here, we investigate how individual energy budgets, phylogeny and habitat structure elasmobranch life history strategies, and how the resulting fast-slow continuum and reproductive strategy framework links to their population performance, demographic resilience and conservation biology[2,13]. We parameterise Dynamic Energy Budget Integral Projection Models (DEB-IPMs) for 157 elasmobranch species[22–26]. In DEB-IPMs, an energy budget model describes a species' growth and reproduction, where energy intake is determined by setting an experienced feeding level[27,28]. To identify life history strategies, we (objective 1) calculate, using the parameterised DEB-IPMs, a set of representative life history traits based on schedules of survival, growth and reproduction for a low and a high feeding level. We (objective 2) evaluate the variation in these traits along major axes using a phylogenetically-corrected principal components analysis (PCA). We then (objective 3) assess to what extent phylogenetic ancestry and habitat (water temperature) determine species position along these major axes. Finally, (objective 4) we test whether species position along these axes predicts population growth rate, speed of recovery from perturbations (demographic resilience) and IUCN conservation status.

2. Methods

2.1 Brief description of the DEB-IPM

A DEB-IPM describes the dynamics of a population comprising cohorts of females of different sizes as a result of their survival, growth and reproduction[22,26]. Specifically, denoting the number of females at year *t* by $N(L,t)$ gives the dynamics of the body length number distribution from year *t* to *t*+1 as:

$$N(L',t+1) = \int_{\Omega} \left[D(L',L(t))R\big(L(t)\big) + G(L',L(t))S(L(t))\right]N(L,t)dL \qquad \text{eqn 1}$$

where the closed interval Ω denotes the length domain. The survival function $S(L(t))$ in equation (1) is the probability that an individual of length *L* survives from time *t* to *t* + 1:

$$S(L(t)) = \begin{cases} e^{-\mu_j} & \text{for } L_b \le L < L_p \ \ \& \ \ L \le L_m E(Y)/\kappa\,, \\ e^{-\mu_a} & \text{for } L_p \le L \le L_m \ \ \& \ \ L \le L_m E(Y)/\kappa\,, \\ 0 & \text{otherwise} \end{cases} \qquad \text{eqn 2}$$

where *E*(*Y*) can range from zero (empty gut) to one (full gut), L_b is length at birth, L_p length at puberty and L_m maximum attainable length (Fig. 1). Individuals die from starvation at a body length at which maintenance requirements exceeds the total amount of assimilated energy, which occurs when $L > L_m \cdot E(Y)/\kappa$ and hence, $S\big(L(t)\big) = 0$ (e.g. an individual of length L_m will die of starvation if $E(Y) < \kappa$, where κ is the fraction of assimilated energy allocated to respiration, with $1 - \kappa$ allocated to reproduction [Fig. 1]). Juveniles and adults often have different mortality rates, and thus, juveniles ($L_b \le L < L_p$) that do not die of starvation (i.e. $L \le L_m \cdot E(Y)/\kappa$) have a mortality rate of μ_j and adults ($L_p \le L \le L_m$) that do not die of starvation (i.e. $L \le L_m \cdot E(Y)/\kappa$) have a mortality rate of μ_a (Fig. 1).

In equation (1), the function $G(L',L(t))$ is the probability that an individual of body length *L* at time *t* grows to length *L'* at *t* + 1, conditional on survival, and follows a Gaussian distribution:

$$G(L',L(t)) = \frac{1}{\sqrt{2\pi\sigma_L^2(L(t+1))}} e^{\frac{-(L'-E(L(t+1))^2}{2\sigma_L^2(L(t+1))}} \qquad \text{eqn 3}$$

with the growth realised by a cohort of individuals with length *L*(*t*) equalling:

$$E\big(L(t+1)\big) = \begin{cases} L(t)e^{-r_B} + \left(1 - e^{-r_B}\right)L_m E(Y) & \text{for } L \le L_m E(Y) \\ L(t) & \text{otherwise} \end{cases}, \qquad \text{eqn 4}$$

and the variance in length at time $t + 1$ for a cohort of individuals of length L as:

$$\sigma^2(L(t+1)) = \begin{cases} (1 - e^{-\dot{r}_B})^2 L_m^2 \sigma^2(Y) & \text{for } L \leq L_m E(Y) \\ 0 & \text{otherwise} \end{cases} \qquad \text{eqn 5}$$

where $\sigma(Y)$ is the standard deviation of the expected feeding level, and where $\dot{r}_B$ is the von Bertalanffy growth rate (Fig. 1).

The reproduction function $R(L(t))$ in equation (1) gives the number of offspring produced between time t and $t + 1$ by an individual of length L at time t:

$$R(L(t)) = \begin{cases} 0 & \text{for } L_b \leq L < L_p \\ E(Y) R_m L(t)^2 / L_m^2 & \text{for } L_p \leq L \leq L_m E(Y) \\ \frac{R_m}{1-\kappa}\left[E(Y) L(t)^2 - \frac{\kappa L(t)^3}{L_m}\right] & \text{for } L_m E(Y) < L \leq L_m E(Y)/\kappa \end{cases} \qquad \text{eqn 6}$$

Individuals are mature when they reach puberty at body length L_p and only surviving adults reproduce; thus, only individuals within a cohort of length $L_p \leq L \leq L_m Y/\kappa$ reproduce.

Finally, the probability density function $D(L', L(t))$ gives the probability that the offspring of an individual of body length L are of length L' at time $t + 1$, and hence describes the association between parent and offspring character values:

$$D(L', L(t)) = \begin{cases} 0 & \text{for } L < L_p \\ \frac{1}{\sqrt{2\pi\sigma_{L_b}^2(L(t))}} e^{\frac{-(L' - E_{L_b}(L(t)))^2}{2\sigma_{L_b}^2(L(t))}} & \text{otherwise} \end{cases} \qquad \text{eqn 7}$$

where $E_{L_b}(L(t))$ is the expected size of offspring produced by a cohort of individuals with length $L(t)$, and $\sigma_{L_b}^2(L(t))$ the associated variance. For simplicity, $E_{L_b}(L(t))$ is set to be constant and its associated variance, $\sigma_{L_b}^2(L(t))$ is assumed to be very small.

DEB-IPMs were parameterised (**Error! Reference source not found.**) using the DEBBIES database of e ctotherms for 157 elasmobranch species, from 11 orders and 37 families[26].

2.2 Life history strategies

Nine representative life history traits were calculated based on schedules of survival, growth and reproduction (Table 1)[1,2,13] in MATLAB Version 9.12[29] using the code in Smallegange and Lucas[26] (objective 1). For each species, this was done for a low and high feeding level, $E(Y)$= 0.6 and $E(Y)$= 0.9, respectively. Feeding levels lower than $E(Y)$= 0.6 were not explored because these were too low for individual growth and reproduction to occur for many species. To identify life history strategies

along major axes (objective 2), we performed a varimax-rotated, phylogenetically corrected principal component analysis (pPCA)[30], using the *phy.pca* function in the R library *phytools*[2,30–33]. Traits were log-transformed and scaled to adhere to PCA assumptions (μ= 0 and SD= 1).

To correct for phylogenetic relatedness among species, a pool of 10,000 possible phylogenetic trees were obtained from Stein et al.[34], available at Vertlife.org. These trees represented 500 root node ages combined with 20 scenarios for infilling taxon with no genetic data. We randomly selected twenty trees and ran the pPCA for each, on both the high and low feeding levels (*E(Y)*= 0.6 and *E(Y)*= 0.9). Each rooted phylogenetic tree had its branch lengths scaled proportionally based on time of separation of clades and species, using the *rotl* package[35]. In the tree, branch length informs on phylogenetic relatedness. The pPCA then links the phylogeny to the life-history traits via a modified covariance matrix and estimated Pagel's λ, a scaling parameter for the phylogenetic correlation between species, expected under Brownian motion[36]. Pagel's λ was estimated using the *ape* package[37] and varies between 0 (phylogenetic independence) and 1 (species traits covary proportionally to their shared evolutionary history)[38]. The loadings for each axis were consistent across each of the trees (Appendix: File S1) and Pagel's λ was either consistently above or below our cut-off value of λ>0.25 (Appendix: File S2), above which we assumed the phylogenetic signal is strong for both feeding levels. Therefore, we report results from one single tree, selected at random from the subsample of twenty trees (Appendix: Fig. S1). Three species (*S. hawaiiensis*, *A. narutobiei* and *M. ambigua*) were not in the Vertlife.org database and thus excluded from the phylogenetic tree and analyses. Two species, *E. granulosus* and *A. bovinus*, were removed because they did not have an associated polygon shapefile on the IUCN database (see below). After visual inspection of the PCAs, *S. microcephalus* (Greenland shark) was identified as an outlier and removed, because of its extreme life history trait values compared to all other species in the dataset.

We checked for the influence of phylogeny and body mass on the final structuring of life history strategies (see Jeschke & Kokko for a detailed discussion[39]) by running PCA analyses with and without a correction for phylogeny, and with and without a correction for body mass. Body mass was corrected for by computing the residuals for linear models between the $\log_{10}$-transformed life history traits (Table 1) and the body mass for each species for both the PCA and the pPCA[3,40,41]. Body mass values were extracted from Fishbase[42] using the *rfishbase* package [43]. Where available, we used the maximum mass given on Fishbase. For species without mass records, we employed length-weight relationships to infer the maximum body mass. If the length-weight relationship used a length that was not present in the database, length-length conversions were conducted prior to the length-weight conversion (e.g. converting fork length to pre-caudal length). Data were not available for all species. The total number of species included in each PCA are summarised in Table S1

(Appendix). We assessed the significance of PC axes using Kaiser's criterion, retaining those PC axes with eigenvalues greater than unity[44].

To compare if and how species position changed between the low and high feeding levels, we took the standardised score (z-score) of each principal components for all species in each analysis (n= 63 for *E(Y)*= 0.6, n= 151 for *E(Y)*= 0.9). The standardised scores were plotted only for the 63 species that were in both analyses.

2.3 Effect of phylogenetic ancestry and habitat (water temperature) on life history patterns

For each feeding level, we assessed if habitat and phylogenetic clade elasmobranch life history variation (objective 3). First, we sourced habitat information (water depth and environmental temperature) for each species. For depth, continuous variable 'commonly used depth' was sourced for each species from the Fishbase database[42,43]. If commonly used depth was unavailable, median depth was sourced from the IUCN database[45]. For the continuous variable temperature, we used 'temperature-at-depth' following the methodology of Barrowclift et al.[19]. To this end, shape files containing polygons of the known depth range for each species were taken from the IUCN database[45]. These shapefiles were overlaid onto the International Pacific Research Center's mean annual ocean temperatures across 27 depth levels (0-2000m), based on a dataset from the Argo Project (available at http://apdrc.soest.hawaii.edu/projects/Argo/data/statistics/On_standard_levels/Ensemble_mean/1x1/m00/index.html). Median temperature-at-depth was calculated for each species using values at the nearest depth level to each species' commonly used depth (or the IUCN median depth where commonly used depth was unavailable). For mesotherm species (family *Lamnidae*) a correction factor of 3.5°C was applied to their median temperature.

We tested collinearity between depth, temperature and clade using visual inflation factor (threshold value VIF>10) in the *faraway* R package[46]. Depth, temperature and clade were all colinear. Therefore, we separately assessed the effect of temperature at depth (as the representative variable for habitat) and clade on the PC scores of the first and second axis of the best fitting (p)PCA for each feeding level. We used four general linear models (LMs) for each feeding level, where the predictor variable was either temperature at depth or phylogenetic clade, and the response variable was either PC1 or PC2 score. For each LM, the model assumptions of Gaussian errors, homoscedasticity and collinearity were confirmed by inspecting the probability plots and error structures in R[32,46,47].

2.4 Life history strategies as predictors of population growth rate, demographic resilience and conservation status

We used LMs to test, for each feeding level, if the PC scores (continuous variables) of the first and second axis of the best fitting PCA, and their interaction, predict population growth rate (λ) and demographic resilience across species (objective 4). To calculate λ, we discretised each DEB-IPM (Eqn 1) by dividing the length domain Ω into 200 very small-width discrete bins, resulting in a matrix **A** of size $m \times n$, where m= n= 200, and which dominant eigenvalue equals λ (Table 1). Demographic resilience was calculated as the damping ratio ξ, with $\xi = \lambda/||\lambda_2||$, where λ_2 is the highest subdominant eigenvalue of matrix **A**[48,49]. To assess predictive links between life history strategies and conservation status, global conservation statuses for each species were sourced from the IUCN database[45], where LC indicates Least Concern, NT indicates Near Threatened, VU indicates Vulnerable, EN indicates Endangered, CR indicates Critically Endangered and DD indicates Data Deficient. We used an ordinal regression to assess if PC scores predict species IUCN conservation status (excluding Data Deficient species).

All LMs, ordinal regression analyses and plots[50–53] were performed in R version 4.3.1[32] in Rstudio[54], using the *dplyr* and *tibble* packages for data manipulation[55,56]. For each LM, the model assumptions of Gaussian errors, homoscedasticity and collinearity were confirmed by inspecting the probability plots and error structures in R[32,46,47].

3 Results

3.1 Elasmobranch life history strategies structure along three axes (objective 1 & 2)

At the low feeding level ($E(Y)$= 0.6), we found that elasmobranch life history traits structure along three separate PC axes that cumulatively explain 88.2% of the total variance in life histories (Table 1: PC1: 42.1%, PC2: 31.2%, PC3: 14.9%). Pagel's λ was lower than our cut-off value of 0.25 (Pagel's λ< 0.001) (Table 1), so the phylogenetic signal did not impact the results. Correcting for body mass did not qualitatively change the results either (Appendix: Table S1) and we thus continued with the PCA results. Generation time (T), progressive growth (γ) and mature life expectancy (L_ω) loaded positively onto PC1 (Fig. 2A) (Table 1). As PC1 scores move from negative to positive, individuals increase their allocation to progressive growth and mature life expectancy (longevity) at the expense of population turnover (i.e., greater generation time), suggesting an axis analogous to the fast-slow continuum[4] (Fig. 2A). Degree of iteroparity (S), mean recruitment success (φ) and net reproductive rate (R_0) were loaded positively onto PC2 and retrogressive growth (ρ) negatively (Fig. 2A) (Table 1). These life history traits are all associated with reproductive strategies. Thus, as PC2 scores move from negative

219 to positive, elasmobranchs attain greater lifetime reproductive success while their retrogressive
220 growth decreases (Fig. 2A). Finally, survivorship curve type (H) and mean age at maturity (L_α) were
221 positively and negatively, respectively, loaded onto PC3 (Table 1). This means that as age at maturity
222 increases (high L_α), senescence rates increase (mortality rate increases with age, corresponding to
223 low H).

224 Like the low feeding level, at the high feeding level ($E(Y)$= 0.9), we also found that elasmobranch life
225 history traits structure along three separate pPC axes that cumulatively explain 86.1% of the total
226 variation in life histories (Table 1: pPC1: 43.1%, pPC2: 31.0%, pPC3: 12.0%). Pagel's λ was higher than
227 our cut-off value of 0.25 (Pagel's λ= 0.31), indicating the phylogenetic signal was significant.
228 Correcting for body mass did not qualitatively change the results (Appendix: Table S1) and thus we
229 continued with the pPCA results. Generation time (T), progressive growth (γ), mature life expectancy
230 (L_ω) and age at maturity (L_α) were loaded positively onto PC1 and mean recruitment success (φ)
231 negatively (Fig. 2B) (Table 1). Like the low feeding level, as PC1 score increases, individuals increase
232 their allocation to progressive growth and mature life expectancy at the expense of longer
233 generation times and later maturity. Therefore, again, PC1 most closely represents the fast-slow
234 continuum (Fig. 2B). Degree of iteroparity (S), mean recruitment success (φ) and net reproductive
235 rate (R_0) were loaded positively onto PC2 and retrogressive growth (ρ) negatively, respectively (Fig.
236 2B) (Table 1). As PC2 score increases, elasmobranchs attain greater lifetime reproductive success
237 (iteroparity and net reproductive rate) and an increased number of breeding females (recruitment
238 success), again representing the reproductive strategy axis (Fig. 2B). Only survivorship curve type (H)
239 was loaded positively onto PC3 (Table 1), so for higher PC3 scores, senescence rates decrease
240 (decreasing mortality with age).

241 Comparing the position of each species at each feeding level showed that species move along each
242 PC axis in particular ways (Fig. 2C). For example, at the low feeding level, species that are fast paced
243 but have a low life reproductive strategy score (e.g. *Mobula birostris*), increase mostly in life history
244 speed with increasing feeding level (Fig. 2C: bottom left-hand corner). But, at low feeding level,
245 species that are fast paced and also have a high reproductive strategy (e.g. *Anoxypristis cuspidata*),
246 move to a lower reproductive strategy with an increase in feeding level (Fig. 2C: top left-hand
247 corner). Likewise, species that are slow paced with a low reproductive strategy at low feeding level
248 (e.g. *Beringraja binoculata*), show a higher reproductive strategy as feeding level increases (Fig. 2C:
249 bottom right-hand corner). But species that are slow paced with a high reproductive strategy (e.g.
250 *Prionace glauca*) tend to show a faster life history speed with increasing feeding level (Fig. 2C: top
251 right-hand corner). Together, these shifts create an anticlockwise 'whirlpool' effect as species move
252 across the life history strategy space in response to an increase in feeding level (Fig. 2C).

3.2 Habitat type shapes life history strategies differently for different feeding levels and clades (objective 3)

For the low feeding level *E*(*Y*)= 0.6, neither temperature at depth (p= 0.350) nor clade (p= 0.320) significantly affected species position on the PC1 (fast-slow) axis. Similarly, neither temperature at depth (p= 0.924) nor clade (p= 0.336) significantly affected species position on the PC2 (reproductive strategy) axis.

At the high feeding level *E*(*Y*)= 0.9, phylogenetic clade did not significantly affect PC1 score (fast-slow continuum) (p= 0.445). There was a significant effect of temperature at depth on PC1 score ($F_{1,149}$= 23.93, adjusted-R^2= 0.13, p= <0.001). PC1 scores decreased in value (and pace of life increased) with increasing temperature at depth, indicating faster pace of life in warmer waters (Fig. 3A). PC2 scores (reproductive strategy) decreased with increasing temperature at depth ($F_{1,149}$= 4.86, adjusted-R^2= 0.03, p= 0.029: Fig. 3B). This suggests that across all elasmobranchs, species with lower reproductive outputs occur in warmer waters. PC2 scores were higher for skates than sharks and rays, indicating that skates have a high reproductive output ($F_{2,148}$= 6.97, adjusted-R^2= 0.11, p= <0.001, Fig. 2B).

3.3 Life history strategies as predictors of population performance and IUCN status depends on feeding level (objective 4)

At the low feeding level *E(Y)*= 0.6, population growth rate significantly increased with increasing PC1 scores (fast-slow axis) and increasing PC2 scores (reproductive strategy axis) (Table 2), showing that slower paced species and species with higher reproductive outputs have higher population growth rates (Fig. 4A: e.g. *Raja montagui, Leucoraja ocellata, Squalus acanthias*). Resilience to perturbations (damping ratio) was significantly affected by the interaction between PC1 and PC2 scores (Table 2). Damping ratio significantly increased with both decreasing PC1 scores and increasing PC2 scores, showing that faster paced species with higher reproductive outputs have increased resilience to perturbations (Fig. 4C: e.g. *Scoliodon laticaudus, Urolophus paucimaculatus, Rhizoprionodon acutus*). There was no significant association of PC1 scores, PC2 scores, or their interaction on the IUCN category of species in the model (Table 2, Fig. 4E).

At the high feeding level *E(Y)*= 0.9, population growth rate was significantly affected by the interaction between PC1 scores (fast-slow axis) and PC2 scores (reproductive strategy) (Table 2). Population growth rate increased with increasing PC2 scores, but this increase was steeper for species with high, negative PC1 scores (faster species) than for species with high, positive PC1 scores (slower species) (Fig. 4B: e.g. *Rostroraja eglanteria, Raja microocellata, Raja montagui*). Resilience to perturbations (damping ratio) was significantly affected by the interaction between PC1 scores and PC2 scores (Table 2). Resilience to perturbations increased with decreasing PC1 (increasing pace of

life) at a higher rate at low PC2 scores than at higher PC2 scores (Fig. 4D). Overall, faster species with intermediate reproductive outputs show the highest resilience to perturbations (Fig. 4D: e.g. *Scoliodon laticaudus, Rhizoprionodon acutus, Anoxypristis cuspidata*). There was a significant positive association between PC1 scores (fast-slow axis) and IUCN category, but not with PC2 scores or their interaction (Table 2). Species with a higher PC1 score (slower pace of life) were more likely to be in a higher threat category than species with a lower PC1 score (faster pace of life) (Fig. 4F).

4 Discussion

Our aim was to investigate how individual energy budgets, phylogeny and habitat type structure elasmobranch life history variation, and if this structured variation can predict population performance, resilience and conservation biology. Elasmobranch life histories are primarily structured along a fast-slow continuum and reproductive strategy axes at both a low and high feeding level. Interestingly, we found that as feeding level increased, species moved along the life history axes in an anticlockwise manner. Regardless, the two life history strategies (the fast-slow continuum and reproductive strategy) predicted species' population growth rate and demographic resilience for both feeding levels, and IUCN conservation status in the higher feeding level.

4.1 The impact of feeding level on quantifying and applying life history strategies

Typically, most of the variation in animal life history strategies, including the elasmobranchs studied here, is captured with two axes: the fast-slow continuum and reproductive strategy axis[2–4]. For many taxa, including elasmobranchs, these life history strategies are influenced by phylogeny and habitat[1], likely due to distinct environmental selective pressures. In this study, we also captured the phenomenon that species move in life history space in an anticlockwise 'whirlpool' manner as their feeding level changes. Specifically, as feeding levels increase, faster-paced species (on the fast end of the fast-slow continuum) with low reproductive output speed up, whilst those with high reproductive output shift to lower reproductive output. Slower-paced species with low reproductive output increase their reproductive output whilst those with high reproductive output increase their pace of life. The exact mechanism that underpins this 'whirlpool' effect is not immediately obvious but possibly related to each species-specific energy budget structure. Such plasticity in life history strategies can be adaptive when developing organisms adjust their allocation decisions in response to their local (feeding) environment, following evolved rules that maximise expected fitness in different ecological conditions[57]. Crucially, the consequences of such feeding level effects can be far-reaching. Like other studies[2,13], we found that the two life history strategy axes predict species population performance, resilience and even conservation status. But the plasticity in life history strategies highlights how predictions on performance, resilience and conservation status *specific to a*

species will depend on its feeding level, and thus, the environment it lives in. One should therefore be cautious when extrapolating how species-specific life history strategies predict their response to (climate) change and perturbations in one environment, to another.

Although we find qualitatively the same two life history strategy axes as in other studies (Appendix: Table S2)[2,5,13,49], there is one notable difference in the life history traits that comprise these life history strategies. One would expect that investment into development, i.e. high progressive growth, is characteristic of species with a faster life history speed. But in our analyses, progressive growth was higher for species with slower life history speeds, not faster (e.g.[2,13]) (Appendix: Table S2). We surmise that this result is due to high variation in the von Bertalanffy growth rate between species that drives a positive correlation between generation time and progressive growth (cf.[58]). For example, the values of progressive growth and generation time change with different values of von Bertalanffy growth rate and feeding level. The relationship between generation time and progressive growth for the reef manta ray, *Mobula alfredi,* can be plotted for a range of feeding levels and values of von Bertalanffy growth rate (Appendix: Fig. S2). For the same von Bertalanffy growth rate value, generation time increases with decreasing feeding level and progressive growth decreases. At the same time, generation time decreases with increasing von Bertalanffy growth rate values. The result is that, at the same feeding level (black solid lines in Appendix: Fig. S2), progressive growth increases with decreasing values of the von Bertalanffy growth rate, and at the same time, generation time increases. Because our dataset covers a wide range of von Bertalanffy growth rate values, this would explain why we found that the slower a species' life history speed, the higher its apparent progressive growth. These findings highlight the need for careful interpretation of correlations between life history traits calculated from demographic datasets (our objective 1 and e.g.[1,2,5,13,31]), and how these are used to predict population characteristics[58].

4.2 Consequences for elasmobranch conservation

For many oceanic species, demographic data are sparce or lacking[59–61]. This often means that the only measure available to evaluate a species relative risk to perturbations like fishing or environmental change, is an estimate of its maximum intrinsic rate of population increase, r_{max}[61–64]. Typically, species with higher (or lower) r_{max} values are assumed to have higher (or lower) resilience to perturbations (cf.[61,65,66]). The intrinsic rate of population increase, r, is related to the population growth rate ($\lambda = e^r$). We found that species with the highest population growth rates do not necessarily show the highest resilience. In fact, particularly at high feeding level, those species where populations grow at a relatively low rate, show the highest resilience. This highlights how it is important to exercise caution when using summary metrics such as r_{max} to predict a species'

resilience [cf.[67]]. Our approach presents a more mechanistic methodology that can be applied to data-sparce elasmobranchs to understand and predict their resilience and conservation status. For example, we found that faster-paced elasmobranchs show higher resilience. We also found that these faster-paced species generally live in warmer waters. Faster paced elasmobranchs might thus be better able to deal with the current rise in sea temperatures than slower species[68,69]. However, some species living in warmer, shallower waters are more intrinsically vulnerable to exploitation (based on their r_{max} values)[19], and may experience higher mortality due to their proximity to densely populated areas with fisheries[70,71] compared to those living in colder and deeper waters[72]. What is more, global (sea water) warming is linked to poorer hunting performance in sharks[73]. Warming can thus reduce the sharks' experienced feeding levels, their population growth rate and ultimately their resilience. Understanding how elasmobranch life histories, their habitats and feeding translate into differences in resilience is crucial to improve management decisions and predict elasmobranch conservation status. Given that the most immediate threat to sharks, skates and rays is overfishing[72,74,75], further study using an energy budget, demographic approach like ours could examine the effects of different fisheries mortalities (either by empirical measures or by derived estimates[76]) on population performance of threatened or highly fished species.

4.3 Conclusion

Many studies have shown that population responses to future environmental change and perturbations depend on the species-specific life-history strategy. Our analyses reveal that feeding level can alter a population's life history strategy; such plasticity in life history strategies will impact how the fast-slow continuum and reproductive strategy framework can be used to predict population responses to change and perturbations. For elasmobranchs, we also provide strong support for the expansion of the classical use of maximum intrinsic rate of population increase, r_{max}, to the fast-slow continuum and reproductive strategy framework, and highlight how our approach can be used to explore different scenarios of (over)fishing to quantify sustainable levels of exploitation. Further research should explore if variations in environmental conditions fuel plasticity of life history strategies in a range of taxa, and how these ultimately impact population performance and responses to change.

Author contributions

Sol Lucas: Conceptualisation, Methodology, Formal analysis, Investigation, Validation, Data curation, Writing- Original draft preparation, Writing- Review & Editing, Visualisation; Per Berggren: Writing- Reviewing and Editing, Supervision; Ellen Barrowclift: Methodology, Formal analysis, Writing- Reviewing and Editing; Isabel M. Smallegange: Conceptualisation, Methodology, Formal analysis,

Investigation, Validation, Data curation, Writing- Original draft preparation, Writing- Review & Editing, Visualisation, Supervision.

Declaration of competing interest

The authors declare no competing interests.

Additional Information

Supplementary information, including data and analysis code used to run the models in MATLAB and RStudio, are available at Figshare (DOI: https://doi.org/10.6084/m9.figshare.26166427).

Acknowledgements

SL was funded by the Leverhulme Doctoral Scholarship in Behaviour Informatics (DS-2017-015).

References

1. Capdevila, P. *et al.* Longevity, body dimension and reproductive mode drive differences in aquatic versus terrestrial life-history strategies. *Funct Ecol* **34**, 1613–1625 (2020).

2. Salguero-Gómez, R. *et al.* Fast–slow continuum and reproductive strategies structure plant life-history variation worldwide. *Proc Natl Acad Sci U S A* **113**, 230–235 (2016).

3. Gaillard, A. J. *et al.* An Analysis of Demographic Tactics in Birds and Mammals. **56**, 59–76 (1989).

4. Gaillard, J. M. *et al.* Life Histories, Axes of Variation in. *Encyclopedia of Evolutionary Biology* 312–323 (2016) doi:10.1016/B978-0-12-800049-6.00085-8.

5. Healy, K., Ezard, T. H. G., Jones, O. R., Salguero-Gómez, R. & Buckley, Y. M. Animal life history is shaped by the pace of life and the distribution of age-specific mortality and reproduction. *Nat Ecol Evol* **3**, 1217–1224 (2019).

6. Stearns, S. C. The Influence of Size and Phylogeny on Patterns of Covariation among Life-History Traits in the Mammals. *Oikos* **41**, 173–187 (1983).

7. Gadgil, M. *et al.* Life Historical Consequences of Natural Selection. *Am Nat* **104**, 1–24 (1970).

8. Reznick, D. The Structure of Guppy Life Histories: The Tradeoff between Growth and Reproduction. *Ecology* **64**, 862–873 (1983).

9. Williams, G. C. Natural Selection, the Costs of Reproduction, and a Refinement of Lack ’s Principle. *Am Nat* **100**, 687–690 (1966).

10. Gamelon, M. *et al.* Effects of pulsed resources on the dynamics of seed consumer populations: a comparative demographic study in wild boar. *Ecosphere* **12**, (2021).

11. Nilsen, E. B. *et al.* A slow life in hell or a fast life in heaven: Demographic analyses of contrasting roe deer populations. *Journal of Animal Ecology* **78**, 585–594 (2009).

12. Rademaker, M., van Leeuwen, A. & Smallegange, I. M. Why we cannot always expect life history strategies to directly inform on sensitivity to environmental change. *Journal of Animal Ecology* 348–366 (2024) doi:10.1111/1365-2656.14050.

13. Salguero-Gómez, R. Applications of the fast–slow continuum and reproductive strategy framework of plant life histories. *New Phytologist* **213**, 1618–1624 (2017).

14. Romeijn, J. & Smallegange, I. M. Exploring how the fast-slow pace of life continuum and reproductive strategies structure microorganism life history variation. *bioRxiv* (2022).

15. Ebert, D. A., Dando, M. & Fowler, S. *Sharks of the World: A Complete Guide*. (Princeton University Press, 2021).

16. Nielsen, J. *et al.* Eye lens radiocarbon reveals centuries of longevity in the Greenland shark (Somniosus microcephalus). *Science (1979)* **353**, 702–704 (2016).

17. Carrier, J. C., Pratt, H. L. & Castro, J. I. Reproductive biology of elasmobranchs. in *Biology of Sharks and Their Relatives* (eds. Carrier, J. C., Musick, J. A. & Heithaus, M. R.) 269–286 (CRC Press, 2004). doi:10.1201/9780203491317.ch10.

18. Miller, E., Wails, C. N. & Sulikowski, J. It’s a shark-eat-shark world, but does that make for bigger pups? A comparison between oophagous and non-oophagous viviparous sharks. *Rev Fish Biol Fish* **32**, 1019–1033 (2022).

19. Barrowclift, E. *et al.* Tropical rays are intrinsically more sensitive to overfishing than the temperate skates. *Biol Conserv* **281**, (2023).

20. Pardo, S. A. & Dulvy, N. K. Body mass, temperature, and depth shape the maximum intrinsic rate of population increase in sharks and rays. *Ecol Evol* **12**, 1–11 (2022).

21. Gravel, S., Bigman, J. S., Pardo, S. A., Wong, S. & Dulvy, N. K. Metabolism, population growth, and the fast-slow life history continuum of marine fishes. *Fish and Fisheries* **25**, 349–361 (2024).

22. Smallegange, I. M., Caswell, H., Toorians, M. E. M. & de Roos, A. M. Mechanistic description of population dynamics using dynamic energy budget theory incorporated into integral projection models. *Methods Ecol Evol* **8**, 146–154 (2017).

23. Sousa, T., Domingos, T., Poggiale, J. C. & Kooijman, S. A. L. M. Dynamic energy budget theory restores coherence in biology. *Philosophical Transactions of the Royal Society B: Biological Sciences* **365**, 3413–3428 (2010).

24. Kooijman, S. A. L. M. & Metz, J. A. J. On the dynamics of chemically stressed populations: The deduction of population consequences from effects on individuals. *Ecotoxicol Environ Saf* **8**, 254–274 (1984).

25. Ellner, S. P., Childs, D. Z. & Rees, M. *Data-Driven Modelling of Structured Populations: A Practical Guide to the Integral Projection Model*. (Springer, Cham, Switzerland, 2016).

26. Smallegange, I. M. & Lucas, S. DEBBIES Dataset to study Life Histories across Ectotherms. *Sci Data* **11**, 1–10 (2024).

27. Kooijman, S. A. L. M., Sousa, T., Pecquerie, L., van der Meer, J. & Jager, T. From food-dependent statistics to metabolic parameters, a practical guide to the use of dynamic energy budget theory. *Biological Reviews* **83**, 533–552 (2008).

28. Kooijman, S. A. L. M. *Dynamic Energy and Mass Budgets in Biological Systems*. (Cambridge University Press, 2001). doi:10.1086/420555.

29. The MathWorks Inc. MATLAB. Preprint at https://www.mathworks.com (2022).

30. Revell, L. J. phytools: An R package for phylogenetic comparative biology (and other things). *Methods Ecol Evol* **3**, 217–223 (2012).

31. Paniw, M., Ozgul, A. & Salguero-Gómez, R. Interactive life-history traits predict sensitivity of plants and animals to temporal autocorrelation. *Ecol Lett* **21**, 275–286 (2018).

32. R Core Team. R: A language and environment for statistical computing. *R Foundation for Statistical Computing, Vienna, Austria* https://www.r-project.org/ (2023).

33. Chamberlain, S. A. & Szöcs, E. Taxize: Taxonomic search and retrieval in R. *F1000Res* **2**, 1–30 (2013).

34. Stein, R. W. *et al.* Global priorities for conserving the evolutionary history of sharks, rays and chimaeras. *Nat Ecol Evol* **2**, 288–298 (2018).

35. Michonneau, F., Brown, J. W. & Winter, D. J. rotl: an R package to interact with the Open Tree of Life data. *Methods Ecol Evol* **7**, 1476–1481 (2016).

36. Freckleton, R. P., Harvey, P. H. & Pagel, M. Phylogenetic analysis and comparative data: A test and review of evidence. *American Naturalist* **160**, 712–726 (2002).

37. Paradis, E. & Schliep, K. Ape 5.0: An environment for modern phylogenetics and evolutionary analyses in R. *Bioinformatics* **35**, 526–528 (2019).

38. Revell, L. J. Phylogenetic signal and linear regression on species data. *Methods Ecol Evol* **1**, 319–329 (2010).

39. Jeschke, J. M. & Kokko, H. The roles of body size and phylogeny in fast and slow life histories. *Evol Ecol* **23**, 867–878 (2009).

40. Jolicoeur, P., Pirlot, P., Baron, G. & Stephan, H. Brain structure and correlation patterns in insectivora, chiroptera, and primates. *Syst Biol* **33**, 14–29 (1984).

41. Revell, L. J. Size-correction and principal components for interspecific comparative studies. *Evolution (N Y)* **63**, 3258–3268 (2009).

42. Froese, R. & Pauly, D. FishBase. *World Wide Web electronic publication* www.fishbase.org (2023).

43. Boettiger, C., Lang, D. T. & Wainwright, P. C. Rfishbase: Exploring, manipulating and visualizing FishBase data from R. *J Fish Biol* **81**, 2030–2039 (2012).

44. Kaiser, H. F. The Application of Electronic Computers to Factor Analysis. *Educ Psychol Meas* **20**, 141–151 (1960).

45. IUCN. The IUCN Red List of Threatened Species. *Version 2022-2* https://www.iucnredlist.org (2022).

46. Faraway, J. J. faraway: Functions and Datasets for Books by Julian Faraway. Preprint at https://cran.r-project.org/package=faraway (2022).

47. Lüdecke, D., Ben-Shachar, M., Patil, I., Waggoner, P. & Makowski, D. performance: An R Package for Assessment, Comparison and Testing of Statistical Models. *J Open Source Softw* **6**, 3139 (2021).

48. Caswell, H. *Matrix Population Models: Construction, Analysis and Interpretation*. (Sinauer Associates, Sunderland, MA, USA, 2001).

49. Capdevila, P., Stott, I., Beger, M. & Salguero-Gómez, R. Towards a Comparative Framework of Demographic Resilience. *Trends Ecol Evol* **35**, 776–786 (2020).

50. Wickham, H. *Ggplot2: Elegant Graphics for Data Analysis*. (Springer-Verlag, New York, 2016).

51. Slowikowski, K. ggrepel: Automatically Position Non-Overlapping Text Labels with 'ggplot2'. *R package version 0.9.3* https://github.com/slowkow/ggrepel (2023).

52. Attali, D. & Baker, C. ggExtra: Add Marginal Histograms to 'ggplot2', and More 'ggplot2' Enhancements. (2023).

53. Hijmans, R. J. raster: Geographic Data Analysis and Modeling. R package version 3.6-21 https://rspatial.org/raster (2023).

54. RStudio Team. RStudio: Integrated Development Environment for R. *RStudio, PBC, Boston, MA* http://www.rstudio.com/ (2023).

55. Wickham, H., François, R., Henry, L. & Müller, K. dplyr: A Grammar of Data Manipulation. https://dplyr.tidyverse.org (2022).

56. Müller, K. & Wickham, H. tibble: Simple Data Frames. https://tibble.tidyverse.org/ (2023).

57. Mcnamara, J. M. & Houston, A. I. State-dependent life histories. *Nature* **380**, 215–221 (1996).

58. van Noordwijk, A. J. & de Jong, G. Acquisition and Allocation of Resources: Their Influence on Variation in Life History Tactics. *Am Nat* **128**, 137–142 (1986).

59. Bradshaw, C. J. A., Mollet, H. F. & Meekan, M. G. Inferring population trends for the world's largest fish from mark-recapture estimates of survival. *Journal of Animal Ecology* **76**, 480–489 (2007).

60. Temple, A. J. *et al.* Life-history, exploitation and extinction risk of the data-poor Baraka's whipray (Maculabatis ambigua) in small-scale tropical fisheries. *J Fish Biol* **97**, 708–719 (2020).

61. Pardo, S. A. *et al.* Growth, productivity, and relative extinction risk of a data-sparse devil ray. *Sci Rep* **6**, 1–10 (2016).

62. Myers, R. A. & Fowlow, P. S. Maximum population growth rates and recovery times for Atlantic cod, Gadus morhua. *Fishery bulletin* **95**, 762–772 (1997).

63. Myers, R. A., Bowen, K. G. & Barrowman, N. J. Maximum reproductive rate of fish at low population sizes. *Canadian Journal of Fisheries and Aquatic Sciences* **56**, 2404–2419 (1999).

64. Dulvy, N. K. *et al.* Methods of assessing extinction risk in marine fishes. *Fish and Fisheries* **5**, 255–276 (2004).

65. Pardo, S. A., Kindsvater, H. K., Reynolds, J. D. & Dulvy, N. K. Maximum intrinsic rate of population increase in sharks, rays, and chimaeras: The importance of survival to maturity. *Canadian Journal of Fisheries and Aquatic Sciences* **73**, 1159–1163 (2016).

66. Cortés, E. Perspectives on the intrinsic rate of population growth. *Methods Ecol Evol* **7**, 1136–1145 (2016).

67. Smallegange, I. M., Flotats Avilés, M. & Eustache, K. Unusually Paced Life History Strategies of Marine Megafauna Drive Atypical Sensitivities to Environmental Variability. *Front Mar Sci* **7**, 1–18 (2020).

68. Rosa, R. *et al.* Early-life exposure to climate change impairs tropical shark survival. *Proceedings of the Royal Society B: Biological Sciences* **281**, (2014).

69. Osgood, G. J., White, E. R. & Baum, J. K. Effects of climate-change-driven gradual and acute temperature changes on shark. *Journal of Animal Ecology* **90**, 2547–2559 (2021).

70. Letessier, T. B. *et al.* Remote reefs and seamounts are the last refuges for marine predators across the Indo-Pacific. *PLoS Biol* **17**, 1–20 (2019).

71. Letessier, T. B. *et al.* Divergent responses of pelagic and benthic fish body-size structure to remoteness and protection from humans. *Science (1979)* **383**, 976–982 (2024).

72. Dulvy, N. K. *et al.* Overfishing drives over one-third of all sharks and rays toward a global extinction crisis. *Current Biology* **31**, 4773-4787.e8 (2021).

73. Pistevos, J. C. A., Nagelkerken, I., Rossi, T., Olmos, M. & Connell, S. D. Ocean acidification and global warming impair shark hunting behaviour and growth. *Sci Rep* **5**, 1–10 (2015).

74. Pacoureau, N. *et al.* Half a century of global decline in oceanic sharks and rays. *Nature* **589**, 567–571 (2021).

75. Worm, B. *et al.* Global shark fishing mortality still rising despite widespread regulatory change. *Science (1979)* **383**, 225–230 (2024).

76. Smith, S. E., Au, D. W. & Show, C. Intrinsic rebound potentials of 26 species of Pacific sharks. *Mar Freshw Res* **49**, 663–678 (1998).

77. Caswell, H. Sensitivity Analysis: Matrix Methods in Demography and Ecology. in *Demographic Research Monographs* Chapter 10 (Springer Open, 2019).

78. Tuljapurkar, S., Gaillard, J. M. & Coulson, T. From stochastic environments to life histories and back. *Philosophical Transactions of the Royal Society B: Biological Sciences* **364**, 1499–1509 (2009).

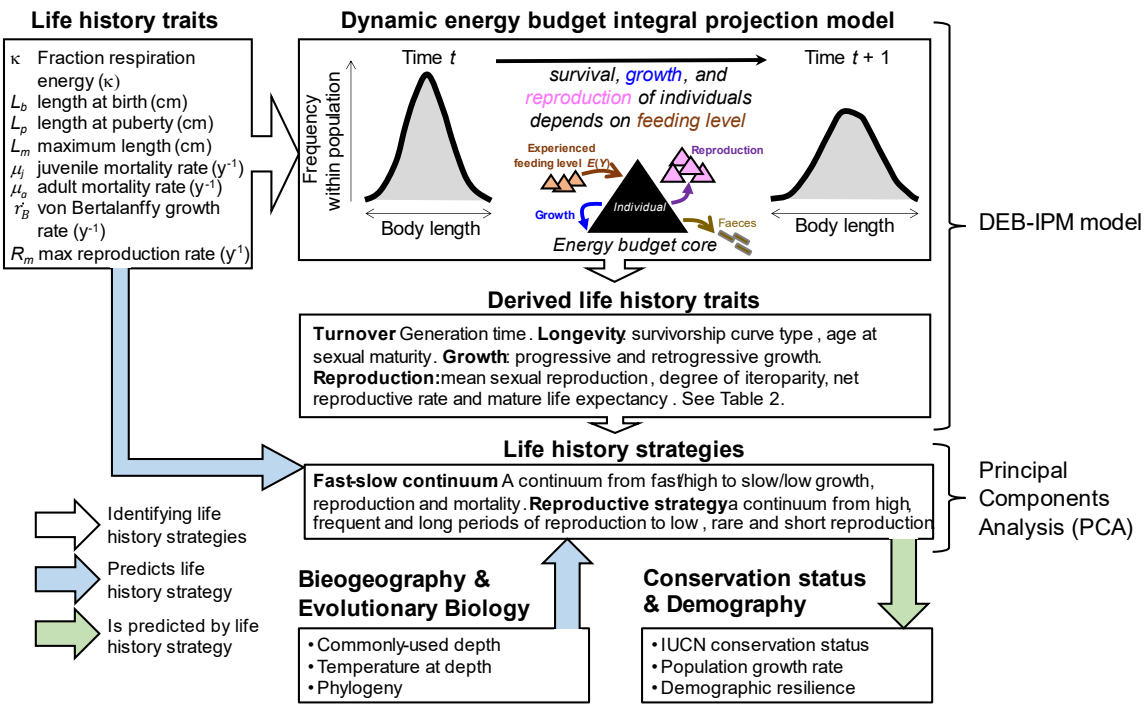

***Figure 1**. Workflow of parameterising a DEB-IPM using the DEBBIES database[26], using the derived life history traits to plot elasmobranch life history strategies in a Principal Components Analysis (PCA). Species biogeography and phylogeny were used to estimate position on PCA axes, and the PC scores were used to predict conservation status, population growth rates and demographic resilience. White arrows indicate parameterisation of models or calculation of traits. Blue arrows represent metrics used to predict life history strategies and green arrows indicate the use of life history strategies to make predictions of conservation status and demography.*

Table 1. Demographic quantities and their loadings onto the Principal Components axes. To calculate life history traits, we discretised each DEB-IPM (Eqn 1) by dividing the length domain Ω into 200 very small-width discrete bins, resulting in a matrix **A** of size $m \times n$, where $m = n = 200$, and which dominant eigenvalue equals λ. Mean lifetime reproductive success R_0 is the dominant eigenvalue of the matrix $\mathbf{F} = \mathbf{V}(\mathbf{I} - \mathbf{GS})^{-1}$, where **I** is the identity matrix and **V**= **DR**, with **D** as the parent-offspring association, **R** the reproduction, **G** the growth and **S** the survival matrix[48]; this gives generation time $T = \log(R_0)/\log(\lambda)$ (Caswell 2001[48]). The mean life expectancy, η_e, is calculated as $\eta_e = 1^T\mathbf{N}$, where 1 is a vector of ones of length m and **N** is the fundamental matrix $\mathbf{N} = (\mathbf{I} - \mathbf{S})^{-1}$. The longevity of an individual of length L is η_L, which means we can calculate age at sexual maturity $\boldsymbol{L_\alpha} = \boldsymbol{\eta_{L_b}}$ and mature life expectancy $\boldsymbol{L_\varpi} = \boldsymbol{\eta_{L_p}}$ so that $\boldsymbol{\eta_e} = \boldsymbol{L_\alpha} + \boldsymbol{L_\varpi}$ (Caswell 2018[77], eqn 4.21). l_x is the probability of surviving to age at least x, and m_x is the average fertility of age class x (cf. Tuljapurkar et al. 2009[78]), $\overline{\mathbf{G}}$ is the mean of G, $\overline{\mathbf{V}}$ is the mean of V, and i and j are the row and column entries of the matrix, respectively. The vital rates included in the studied set of demographic quantities (progressive growth γ, retrogressive growth ρ, and sexual reproduction φ) were averaged across the columns j (the length bins), weighted by the relative contributions of each stage at stationary equilibrium. For example, to calculate mean sexual reproduction φ, we summed the values in the columns j of the **V** matrix and multiplied each φ_{ij} by the corresponding jth element w_j of the stable stage distribution w, calculated as the right eigenvector of **A**.

		Feeding level		*E(Y)*= 0.6			*E(Y)*= 0.9		
		Number of species in analysis		63			151		
Demographic quantity	**Symbol**	**Definition**	**Equation**	**PC1**	**PC2**	**PC3**	**p-PC1**	**p-PC2**	**p-PC3**
Generation time	T	Number of days required for the individuals of a population to be fully replaced by new ones	$T = \frac{\log(R_0)}{\log(\lambda)}$	**0.532**	-0.215	-0.007	**0.942**	-0.234	0.147
Survivorship curve	H	Keyfitz' entropy (H < 1 denotes increasing mortality rate with age, H > 1 denotes decreasing mortality rate with age,(H)= 1 denotes a constant mortality rate with age) (Keyfitz & Caswell 2005).	$H = -\frac{\sum_{x=0}^{x=\eta_e} \log(l_x) l_x}{\sum_{x=0}^{x=\eta_e} l_x}$	0.281	0.110	**0.772**	0.086	0.083	**0.987**
Age at maturity	L_α	Number of days that it takes an average individual in the population to become reproductive	$L_\alpha = \eta_{L_b}$	0.274	0.048	**-0.538**	**0.828**	0.384	-0.228
Progressive growth	γ	Mean probability of growing to a larger length across the length domain Ω.	$\gamma = \sum_i^m \overline{\mathbf{G}}_{i,j}\|_{i<j}$	**0.511**	0.006	-0.007	**0.869**	-0.004	0.043
Retrogressive growth	ρ	Mean probability of growing to a smaller length across the length domain Ω.	$\rho = \sum_i^m \overline{\mathbf{G}}_{i,j}\|_{i>j}$	-0.161	**-0.462**	0.042	-0.138	**-0.898**	-0.066
Mean recruitment success	φ	Mean per-capita number of recruits across the length domain Ω.	$\varphi = \sum_i^m \overline{\mathbf{V}}_{i,j}$	-0.210	**0.521**	0.043	**-0.720**	**0.643**	0.092
Degree of iteroparity	S	Coefficient of variation in age at reproduction	$S = \overline{m}_x / \sigma(m_x)$	-0.045	**0.451**	0.169	-0.228	**0.734**	0.059
Net reproductive rate	R_0	Mean number of recruits produced during the mean life expectancy of an individual in the population.	$R_0 = \sum_{x=0}^{x=\eta_e} l_x m_x$	0.097	**0.474**	-0.287	0.344	**0.870**	-0.028
Mature life expectancy	L_ω	Number of days from the mean age at maturity (L_α) until the mean life expectancy (η_e) of an individual in the population.	$\boldsymbol{L_\varpi} = \boldsymbol{\eta_{L_p}}$	**0.469**	0.162	-0.023	**0.899**	0.264	0.187
		Axis		**Fast-slow**	**Repro**	**Longevity**	**Fast-slow**	**Repro**	**Longevity**
		Proportion of variance explained		42.1%	31.2%	14.9%	43.1%	31.0%	12.0%
		Cumulative proportion of variance explained		42.1%	73.3%	88.2%	43.1%	74.1%	86.1%
		Kaiser criterion		3.79	2.80	1.34	15.05	7.78	1.17
		Pagel's lambda (for the pPCA)				-		0.303	

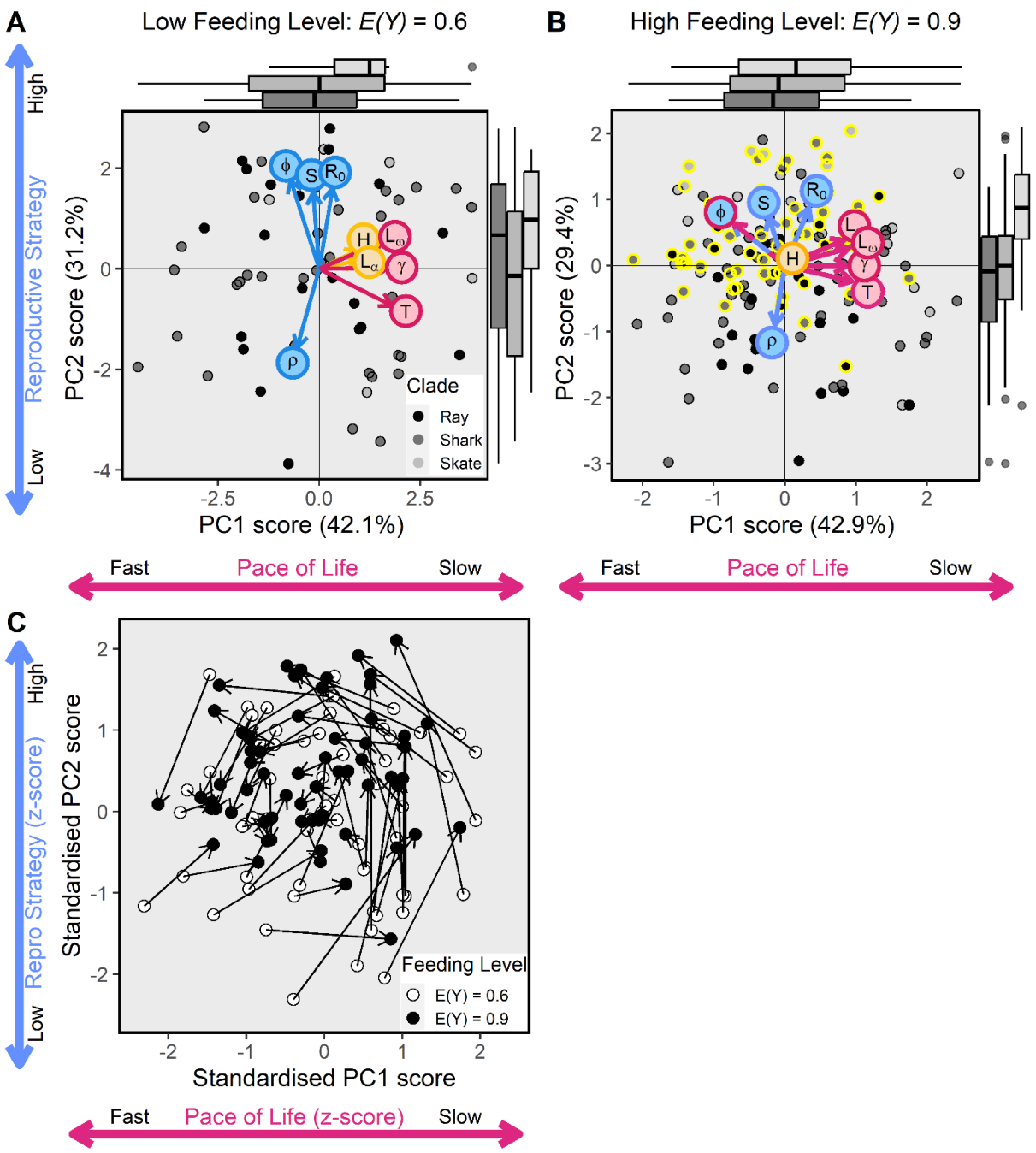

Figure 2. *(p)PCA plots for the 0.6 (A) and 0.9 (B) feeding levels, representing 63 and 151 species respectively. Marginal boxplots of the split by clade (Shark, Skate and Ray) are included for each principal component. Species present in A are highlighted in yellow in B. Labelled arrows correspond to the variables used in the PCA analysis and show the magnitude and direction of the loadings. Red arrows align with the fast-slow continuum, blue arrows align with the reproductive axis and the orange arrow does not align with either of the primary two principal components. The dashed blue/red arrow aligns with both the Slow-Fast continuum and the reproductive axis in plot B. (C) the change standardised (z-scored) PC scores plotted for the 63 species in both low (white points) and high (black points) feeding level. The change in life history strategies between low and high feeding level creates a 'whirlpool' effect.*

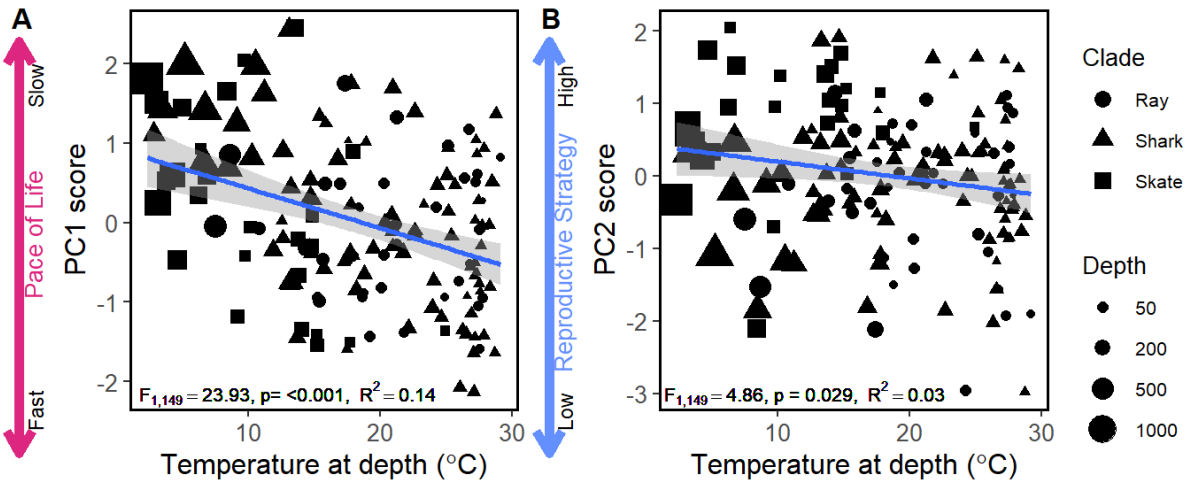

Figure 3. *For the high feeding level E(Y)= 0.9. (A): The relationship between temperature-at-depth and PC1 (fast slow axis). Warmer temperatures relate to negative PC1 scores (faster paces of life). (B) PC2 score decreased for increasing temperature-at-depth. Reproductive output was greater for species inhabiting cooler waters. F-statistics, p-values and R^2 for each analysis are in each plot window. The grey band around the fitted models shows the 95% confidence intervals.*

Table 2. General linear models for population growth rate (λ) and demographic resilience (damping ratio, ξ), as well as ordinal regression models for IUCN conservation status, as a response to PC1 (fast-slow axis) and PC2 (reproductive strategy) scores, for both the low (*E(Y)*=0.6) and high (*E(Y)*=0.9) feeding levels.

Variable	Axes	Estimate	df	Std. Error	p	R^2
		Feeding Level E(Y)= 0.6				
λ ~ *PC1 * PC2*	Intercept	1.010		0.008	**<0.001**	0.674
	PC1	0.042	1	0.004	**<0.001**	
	PC2	0.031	1	0.005	**<0.001**	
	PC1:PC2	0.002	1	0.003	0.402	
	Error term	0.067	59			
ξ ~ *PC1 * PC2*	Intercept	1.164		0.011	**<0.001**	0.590
	PC1	-0.034	1	0.006	**<0.001**	
	PC2	0.053	1	0.007	**<0.001**	
	PC1:PC2	-0.009	1	0.004	**0.029**	
	Error term	0.092	59			
as.factor(IUCN) ~ PC1 * PC2	PC1	0.019		0.116	0.869	0.012
	PC2	-0.128		0.133	0.336	
	PC1:PC2	0.088		0.073	0.227	
		Feeding Level E(Y)= 0.9				
λ ~ *PC1 * PC2*	Intercept	1.215		0.007	**<0.001**	0.826
	PC1	-0.068	1	0.007	**<0.001**	
	PC2	0.167	1	0.007	**<0.001**	
	PC1:PC2	-0.082	1	0.007	**<0.001**	
	Error term	0.086	147			
ξ ~ *PC1 * PC2*	Intercept	1.237		0.012	**<0.001**	0.544
	PC1	-0.151	1	0.013	**<0.001**	
	PC2	-0.041	1	0.013	**0.001**	
	PC1:PC2	0.037	1	0.013	**0.004**	
	Error term	0.151	147			
as.factor(IUCN) ~ PC1 * PC2	PC1	0.483		0.151	**0.001**	0.030
	PC2	-0.095		0.150	0.526	
	PC1:PC2	-0.160		0.150	0.287	

R^2 values are adjusted-R^2 for the linear models and pseudo-R^2 for the ordinal regression on conservation status. McFadden's pseudo R^2 was calculated for the ordinal regression models using the equation $R^2 = 1 - \frac{residual\ deviance}{null\ deviance}$.

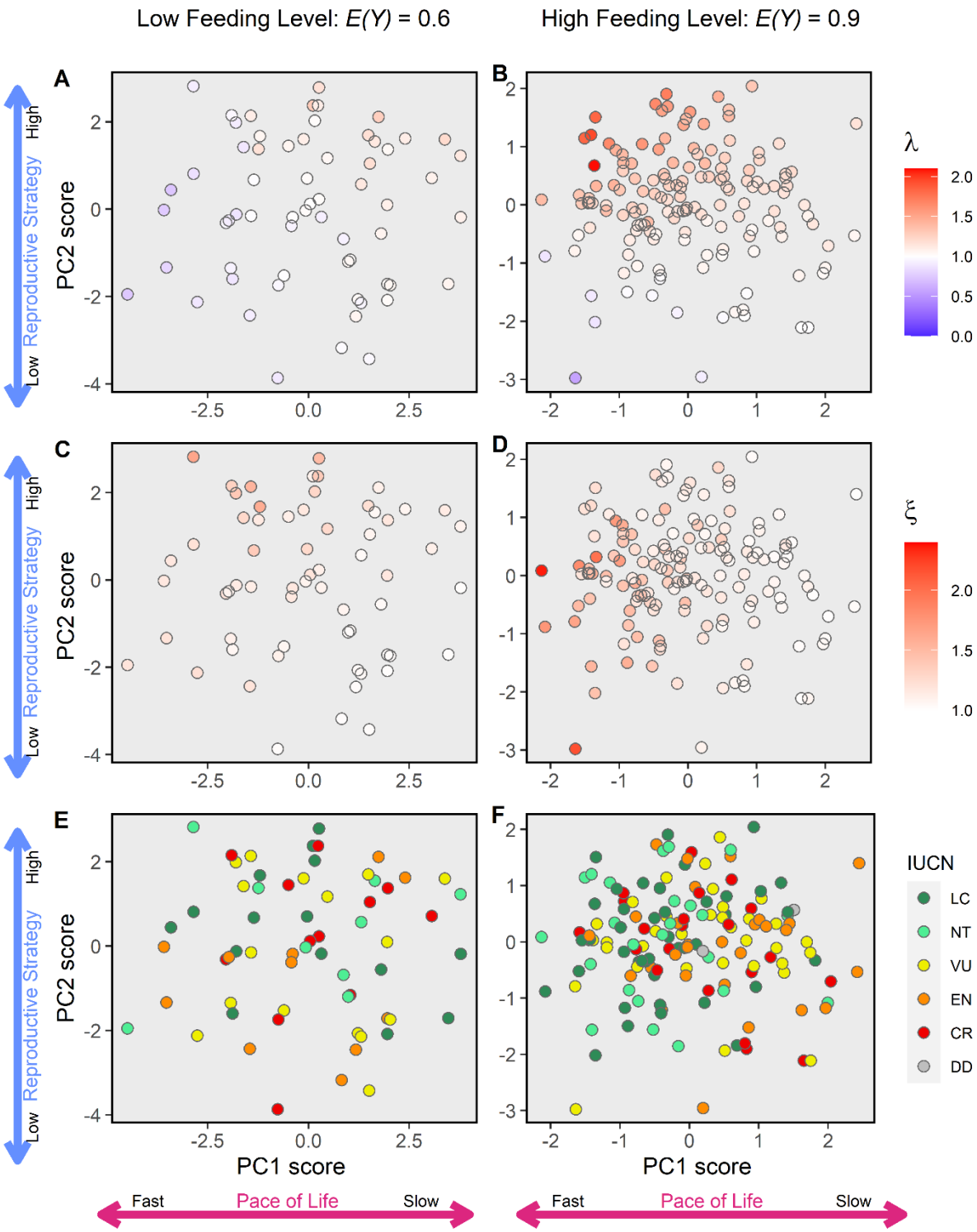

Figure 4. *Overlays on the PCA figures for both feeding levels: E(Y)= 0.6 (A,C,E) and E(Y)= 0.9 (B,D,F). Population growth rate (A,B), damping ratio (C,D), IUCN conservation status (E,F).*